Guiding chemical pulses through geometry: Y junctions

L. Qiao and I. G. Kevrekidis*
Department of Chemical Engineering, Princeton University, Princeton, New Jersey 08544, USA

C. Punckt and H. H. Rotermund
Fritz-Haber-Institut der MPG, Faradyweg 4-6, 14195 Berlin, Germany
(Received 8 December 2005; published 29 March 2006)

We study computationally and experimentally the propagation of chemical pulses in complex geometries. The reaction of interest, CO oxidation, takes place on single crystal Pt(110) surfaces that are microlithographically patterned; they are also *addressable* through a focused laser beam, manipulated through galvanometer mirrors, capable of locally altering the crystal temperature and thus affecting pulse propagation. We focus on sudden changes in the domain shape (corners in a Y-junction geometry) that can affect the pulse dynamics; we also show how brief, localized temperature perturbations can be used to control reactive pulse propagation. The computational results are corroborated through experimental studies in which the pulses are visualized using reflection anisotropy microscopy.

DOI: 10.1103/PhysRevE.73.036219 PACS number(s): 05.45.−a, 82.40.Ck, 82.40.Np

I. INTRODUCTION

Reaction control is an essential task in the chemical process industry; it can stabilize unstable (but profitable) operating states, and, in a multiobjective context, can enhance reactor performance while satisfying safety and environmental constraints. Non-steady-state (e.g., periodic) operation may result in better average productivity or selectivity than steady-state operation [as suggested in the early 1960s in the pioneering work of F. Horn (see Ref. [1] and references therein)]. At a much finer scale, the nonlinear characteristics of heterogeneous catalytic reactions on single-crystal catalysts could be exploited to improve overall yield and selectivity through spatiotemporally resolved actuation [2,3]. Microlithography, by designing the shape of reactive domains as well as prescribing the geometry and statistics of heterogeneous inclusions, provides a different avenue of "talking" to the local dynamics of catalytic reactions (e.g., Ref. [4]). The phenomenology of pattern formation on microcomposite catalytic surfaces can be much richer than that in uniform media. There have been extensive experimental and computational studies in this area, both from our group [5–14] and in the work of others [15–17]. For the low-pressure CO oxidation on Pt(110), the heterogeneities deposited onto the catalytic Pt surface can be either inert, such as TiO_2, or may consist of different active catalysts for the reaction, e.g., metals like Rh and Pd. Such fields of heterogeneous inclusions affect the reaction dynamics and the formation of patterns on the catalytic Pt surface largely through their interfaces.

The heterogeneity in such composite catalysts is solely spatial; their geometry is determined upon construction and does not change with time. In more recent studies, spatiotemporal forcing (using a galvanometer mirror-manipulated focused laser beam) was applied during CO oxidation on a Pt(110) single crystal [2]. Pulses and fronts, the basic building blocks of patterns, could be formed, guided, and destroyed with an addressable laser beam; the addressability function was also used to enhance catalytic reactivity in Ref. [3].

From the implementation of chemical "logical gates" (e.g., Ref. [18]) to the recent spatiotemporal control of morphogenetic patterns in drosophila embryos [19], and from drop formation control in microfluidics [20] to the guidance of matter waves in Bose-Einstein condensates [21], guiding pulses and fronts in complex geometries is an essential task in spatiotemporal pattern control. What makes it increasingly possible is the combination of spatiotemporally finely resolved sensing combined with spatiotemporally finely resolved actuation. Whether the pattern-forming system is naturally photosensitive, like the chemical waves in Ref. [22], or rendered photosensitive, like the neurons in Ref. [23] through genetic manipulation, rapid technological developments in finely resolved optical actuation techniques (e.g., see Ref. [24]) are rapidly and radically changing the experimental exploration and control of spatiotemporal pattern formation.

In this paper, we explore the combined effects of geometry and of spatiotemporally resolved addressability. In particular, we explore the influence of inert boundary geometry on the dynamics of propagating pulses for CO oxidation on a microcomposite Pt(110) surface, and show how these dynamics can be altered using an addressable laser beam. Our geometry of choice for pulse propagation studies is a Y-shaped junction structure, in which sharp boundary curvature changes (corners) can effectively dictate pulse propagation. We systematically explore the effect of varying the junction geometry on reactive pulse propagation; a related rhomb geometry is also studied, leading to qualitatively similar results. We then show how one can *actively* alter the phenomena dictated by geometry through the use of single-shot spatiotemporally localized laser heating. The computational predictions are validated by experimental observations of reactive pulses visualized through reflection anisotropy microscopy (RAM) [25].

*Also at the Program in Applied and Computational Mathematics (PACM), Princeton University, Princeton, NJ 08544.

II. MODELING

In our simulations, we use the three-variable Krischer-Eiswirth-Ertl reaction-diffusion model for CO oxidation on Pt(110) with a surface phase transition described in Ref. [26]. This surface reaction follows a Langmuir-Hinshelwood mechanism,

$$\mathrm{CO} + * \leftrightharpoons \mathrm{CO}_{\mathrm{ads}},$$

$$2* + \mathrm{O}_2 \rightarrow 2\mathrm{O}_{\mathrm{ads}},$$

$$\mathrm{CO}_{\mathrm{ads}} + \mathrm{O}_{\mathrm{ads}} \rightarrow 2* + \mathrm{CO}_2\uparrow,$$

accompanied by a $1\times2\rightarrow1\times1$ phase transition of the Pt(110) surface due to CO adsorption. When the coverage of CO lies between 0.2 and 0.5, the fraction of the 1×1 surface increases monotonically as the CO coverage increases. The sticking coefficient of oxygen is 50% higher on the 1×1 surface as compared to the 1×2 surface. The 1×1 phase favors oxygen adsorption, which leads to reactive consumption of CO. This can lead to oscillatory behavior of the reaction, and also allows the formation of propagating reaction pulses.

The equations for this kinetic model are

$$\dot{u} = k_u s_u p_{co}\left[1 - \left(\frac{u}{u_s}\right)^3\right] - k_1 u - k_2 u v + D_u \nabla^2 u,$$

$$\dot{v} = k_v p_{o_2}[w s_{v_1} + (1-w)s_{v_2}]\left(1 - \frac{u}{u_s} - \frac{v}{v_s}\right)^2 - k_2 u v,$$

$$\dot{w} = k_3[f(u) - w],$$

where by u, v, and w we denote the surface coverage of CO and O, and the surface fraction of 1×1 phase, respectively. The adsorption rate constants for CO and O_2, and k_u and k_v, respectively, are considered to be constant within the temperature range considered here. The rate constants k_1, k_2, and k_3 for the desorption, reaction, and surface phase transition are given by the Arrhenius formula $k_i = k_i^0 \exp(-E_i/kT)$, and T is the temperature of the single crystal. We used the parameters for Pt(110) given in Table II of Ref. [26] as follows:

$$u_s = 1, \quad v_s = 0.8, \quad s_u = 1, \quad s_{v_1} = 0.6, \quad s_{v_2} = 0.4,$$

$$k_u = 3.135 \times 10^5 \ \mathrm{s}^{-1}\ \mathrm{mbar}^{-1},$$

$$k_v = 5.858 \times 10^5 \ \mathrm{s}^{-1}\ \mathrm{mbar}^{-1},$$

$$k_i = k_i^0 \exp(-E_i/kT), \quad i = 1,2,\text{and } 3,$$

$$k_1^0 = 2 \times 10^{16}\ \mathrm{s}^{-1}, \quad E_1 = 38\ \mathrm{kcal/mol},$$

$$k_2^0 = 3 \times 10^{16}\ \mathrm{s}^{-1}, \quad E_2 = 10\ \mathrm{kcal/mol},$$

$$k_3^0 = 10^2\ \mathrm{s}^{-1}, \quad E_3 = 7\ \mathrm{kcal/mol}.$$

We used the diffusion coefficient reported in Ref. [27],

$$D_u = D_u^0 \exp(-E_u/kT),$$

$$D_u^0 = 10^{-4}\ \mathrm{cm}^2/\mathrm{s}, \quad E_u = 7\ \mathrm{kcal/mol}.$$

The function $f(u)$ is fit to experimental data to give the rate of surface phase transition as a function of u, the CO surface coverage, as follows:

$$f(u) = \begin{cases} 0 & \text{for } u \leqslant 0.2, \\ \dfrac{u^3 - 1.05u^2 + 0.3u - 0.026}{-0.0135} & \text{for } 0.2 < u < 0.5, \\ 1 & \text{for } u \geqslant 0.5. \end{cases}$$

For simplicity, the diffusion of CO is taken to be isotropic and no-flux boundary conditions are used in our simulations. To reflect the influence of laser heating on the dynamics of the reaction, we approximate the local temperature increase caused by a laser spot through a local Gaussian temperature field. The heat generated by the reaction ($\sim$1 mW) can be neglected compared to the power of the laser beam ($\sim$1 W). Since the diffusivity of adsorbed CO ($\sim10^{-8}\ \mathrm{cm}^2/\mathrm{s}$) is much smaller than the thermal diffusivity constant of Pt ($\sim10^{-1}\ \mathrm{cm}^2/\mathrm{s}$), we can assume the local Gaussian temperature field is established (vanishes) instantaneously as the laser beam is applied (removed) [28,29]. In our simulations, we use the commercial finite element package FEMLAB to compute the time-dependent evolution of reactive pulses in 2D Y-junction geometries; our meshes typically consisted of $\sim$12000 linear elements.

There exist two types of pulses (O-rich and CO-rich) for CO oxidation on Pt(110) under different reaction conditions [30]. We have used the O-rich pulse for our computations throughout the paper except in Fig. 7. Other than that, a "pulse" refers to an O-rich pulse.

III. COMPUTATIONAL RESULTS

A. Pulse propagation in a Y junction

The geometry of the Y junction structure is described through the parameters W, w, h, α, and θ [see the first snapshot in Fig. 1(a)]. When a reactive pulse reaches the corners of the Y junction that are denoted by the two angles α and θ, the pulse front starts becoming convex. The local traveling speed of the pulse decreases due to this convex curvature [31,32]. When the local curvature required to "go around" one of the corners exceeds a certain limit, the pulse loses stability, "decollates" from the boundary, and -here- disappears [33]. With appropriate angles α and θ, by adjusting the position of the "prow" to the exit (i.e., adjusting h), we can force the pulse to choose none, one, or both of the channels to propagate in (Fig. 1). The behavior of the pulse also depends strongly on the selected partial pressures of CO and O_2. Under reaction conditions for Fig. 1, decreasing the amount of CO in the gas phase stabilizes the pulse. Below some critical value for P_{CO} the pulses will propagate through both channels, essentially independent of the selected geometry.

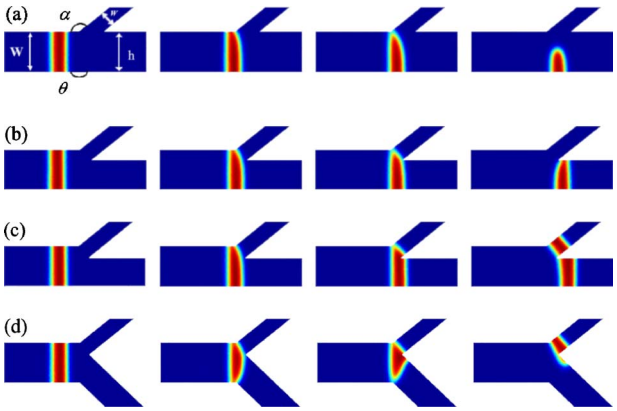

FIG. 1. (Color online) Pulse propagation in different Y junction structures. By choosing appropriate geometric parameters, we are able to dictate the pulse transmission patterns. (a) $h=5$, $\theta=\pi$; (b) $h=3.7$, $\theta=\pi$; (c) $h=3.5$, $\theta=\pi$; (d) $h=3.5$, $\theta=\frac{3}{4}\pi$. Other parameters: $W=5$, $w=1.93$, $\alpha=\frac{7}{9}\pi$, $T=535.5$ K, $P_{CO}=4.95\times10^{-5}$ mbar, $P_{O_2}=2.0\times10^{-4}$ mbar. The unit dimensionless length corresponds to a real length of 3.7 μm throughout the paper except in Fig. 7, where it corresponds to 3.8 μm.

B. Quantifying the geometry-induced instability in reactive pulse propagation

We now begin a quantitative exploration of the geometry-induced instability of pulse propagation in our model system. Junctions between different linear "corridors" are an important building block for complex geometries. The two geometrical parameters characterizing a junction are the width of the channel W and the angle θ at the corner (Fig. 2). When the reaction conditions are fixed, depending on the choice of W and θ, the pulse may or may not be able to pass the corner, as shown in Fig. 3.

When a pulse attempts to turn around a corner, if W is small, the entire pulse becomes curved as a circular arc due to the influence of the no-flux boundaries, and the curvature of the pulse is given by $\frac{1}{r}=\frac{\sin(\pi-\theta)}{W}$. If this geometry-determined curvature becomes larger than a critical value $\frac{1}{r_c}$, a constant determined by the dynamics of the system and the reaction conditions, the pulse becomes unstable and disappears [34]. When W is large, the pulse only curves locally, close to the corner, and further increase in W has little influence on this high local curvature of the pulse. When W is above some critical value (about 6 for curves in Fig. 3), this local curvature of the pulse reaches a minimum and becomes independent of W and only a function of θ. If this minimum value of local curvature is still larger than $\frac{1}{r_c}$, the pulse will decollate from the corner and fail to pass through. We can thus rationalize the existence, for each given set of reaction conditions, of a critical angle below which the pulse cannot propagate around the corner for any W.

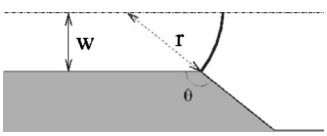

FIG. 2. Geometry of a corner structure, $r=\frac{W}{\sin(\pi-\theta)}$.

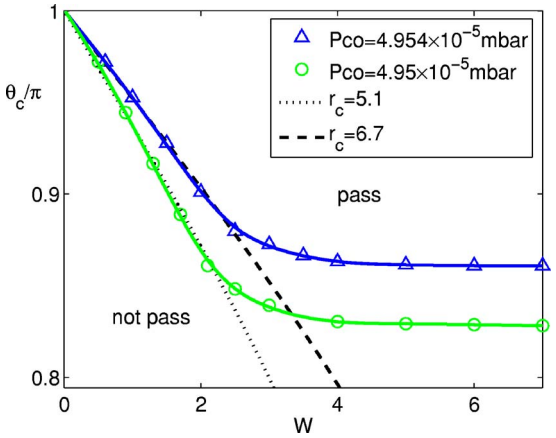

FIG. 3. (Color online) Critical angle θ_c for a pulse to turn around a corner, as a function of dimensionless channel width W. For fixed CO pressure, pulses in a geometry with θ and W chosen "above" the solid lines shown are able to turn around the corner. The solid lines, fitted to data points, are included to guide the eye. The dashed and dotted lines are given by $r_c=\frac{W}{\sin(\pi-\theta_c)}$ for different r_c. $T=535.5$ K, $P_{O_2}=2.0\times10^{-4}$ mbar.

Another geometric structure with features similar to the Y junction is the rhomb constriction, which arises in microcomposite TiO_2/Pt checkerboards (Fig. 4).

The critical angles θ_c (for the Y junction) and ϕ_c (for the rhomb constriction) that allow the pulse to propagate through the structure are plotted as a function of the width W, as in Fig. 5, under the same reaction conditions. The y axis in Fig. 5 for the rhomb constriction structure is chosen to be $(\phi/2+\pi/2)/\pi$, so that the two critical curves correspond (they are almost identical) when W is small (<1). The nonmonotonic decrease of ϕ_c for the rhomb constriction structure can be rationalized by a simple geometric observation: as W increases, the front and back of the pulse are approaching closer and closer to each other at the corner (see the insets in Fig. 5); this can lead to a different mechanism for the decollation of the pulse.

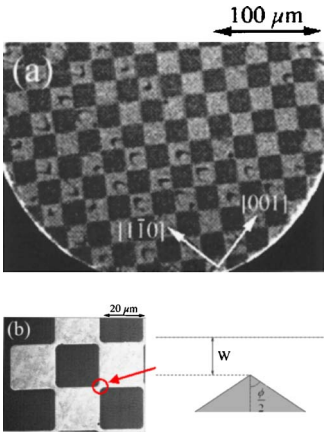

FIG. 4. (Color online) (a) A snapshot showing a microdesigned TiO_2/Pt checkerboard. The inactive TiO_2 rhombs appear black while pulses (little arcs in the first snapshot) are propagating on the light-gray Pt(110) surface. (b) A blow-up of the checkerboard structure. To its right, a geometry (symmetric around the centerline) we used in the simulations of the rhomb constriction is depicted.

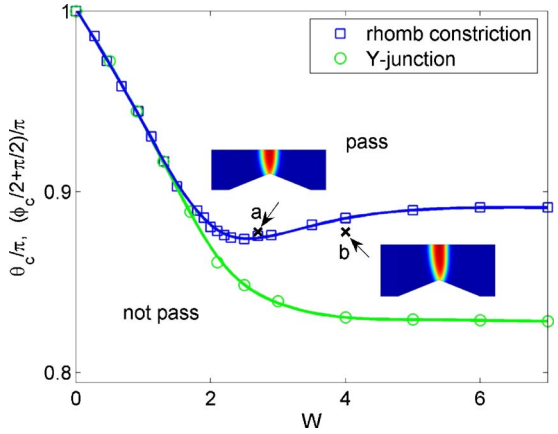

FIG. 5. (Color online) Critical angle for pulse turning around the corner as a function of channel width W for the rhomb constriction and the Y-junction structure. For the rhomb constriction structure, we plot $\phi_c/2+\pi/2$ vs W instead of ϕ_c vs W. For rhomb constriction (Y-junction) structures with values of W and $\phi/2+\pi/2(\theta)$ chosen "above" the corresponding curve, pulses are able to turn around the corner. The solid lines, fitted to data points, are included to guide the eye. Snapshots of a pulse propagating in the rhomb constriction structure at point $a(2.7,0.88)$ and $b(4.0,0.88)$ are shown in the insets. $T=535.5$ K, $P_{CO}=4.95\times10^{-5}$ mbar, $P_{O_2}=2.0\times10^{-4}$ mbar.

C. Pulse manipulation with local laser heating

1. Using the laser to assist pulse propagation

The local increase of temperature caused by a short laser "burst" accelerates the local desorption of CO and may thus assist the propagation of an O-rich pulse. We can therefore use local laser heating to assist the propagation of an O-rich pulse around corners that would be too sharp for the pulse to go through under isothermal conditions.

In Fig. 6, a local increase of temperature [see the high-temperature field close to the corner in Fig. 6(b′)] reignites the CO-poisoned surface, and reattaches the decollated oxygen pulse back toward the corner [close to the corner in Figs. 6(c) and 6(d)]. This result has been confirmed experimentally, as we will see below.

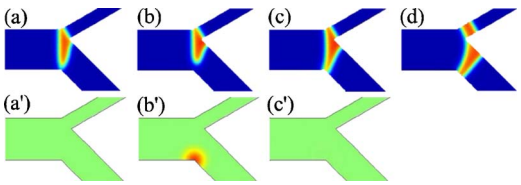

FIG. 6. (Color online) Using local laser heating to assist the propagation of an O-rich pulse around the corner. Snapshots (a)–(d) show the coverage of oxygen; corresponding instantaneous temperature fields before, after [(a′) and (c′), respectively], as well as during the laser shot [(b′)] are plotted in the second row. Laser heating is turned on for a total of 0.4 s (from $t=5.0$ to 5.4 s) and centered at the lower junction corner; the maximum temperature increase there is 3 K. The width of the left channel is 6. (a) $t=4.5$ s, (b) $t=5.0$ s, (c) $t=5.5$ s, (d) $t=8.0$ s. $T=535.5$ K, $P_{CO}=4.95\times10^{-5}$ mbar, $P_{O_2}=2.0\times10^{-4}$ mbar.

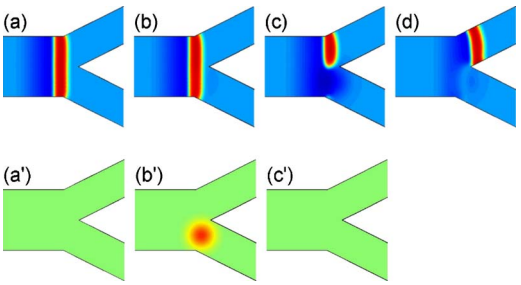

FIG. 7. (Color online) Using local laser heating to prevent the propagation of a CO-rich pulse. Similar to Fig. 6, instantaneous temperature fields [(a′)–(c′)] are plotted below the corresponding CO coverage [(a)–(c)]. The local laser heating is turned on for a total of 1 s (from $t=12$ to 13 s) and centered in the middle of the lower channel entrance with a maximum temperature increase of 5 K. The width of the left channel is 20. (a) $t=11$ s, (b) $t=12$ s, (c) $t=13$ s, (d) $t=17$ s. $T=540$ K, $P_{CO}=4.2\times10^{-5}$ mbar, $P_{O_2}=1.33\times10^{-4}$ mbar.

2. Using the laser to prevent pulse propagation

Laser heating can also be used to eliminate a pulse. We already know that temperature increase shifts the balance toward the desorption of CO. If we apply local laser heating to a CO-rich pulse, it causes CO to desorb locally so that part of the pulse is "removed," as shown in Fig. 7. This phenomenon has also been observed in experiments, as we will show later.

Local laser heating can also prevent the propagation of O-rich pulses through a different mechanism. In Fig. 8, we first apply local laser heating for a short time to locally ignite the CO-poisoned catalytic surface far ahead from the pulse without creating a new pulse [Figs. 8(b) and 8(c)]. The local surface then slowly reverts to the quenched steady state after the laser heating is turned off [as in Fig. 8(d)]. There exists a refractory period before this area of the surface can be reignited, because the dynamics of the Pt phase reconstruction are slow. The arriving O-rich pulse propagates before the local surface recovers; it may not propagate through this area; it "evaporates" [see Figs. 8(e) and 8(f)].

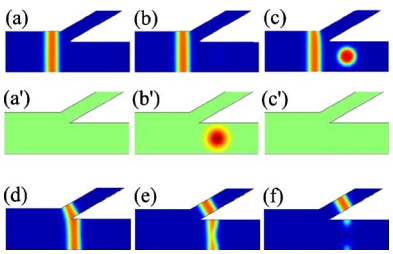

FIG. 8. (Color online) Using local laser heating to prevent the propagation of an O-rich pulse. The local laser heating is turned on for a total of 0.4 s (from $t=1.5$ to 1.9 s) and centered in the middle of the lower channel entrance with a maximum temperature increase of 4.5 K. The width of the left channel is 6. (a) $t=1.0$ s, (b) $t=1.5$ s, (c) $t=2.0$ s, (d) $t=7.0$ s, (e) $t=10.0$ s, (f) $t=12.0$ s. $T=535.5$ K, $P_{CO}=4.95\times10^{-5}$ mbar, $P_{O_2}=2.0\times10^{-4}$ mbar.

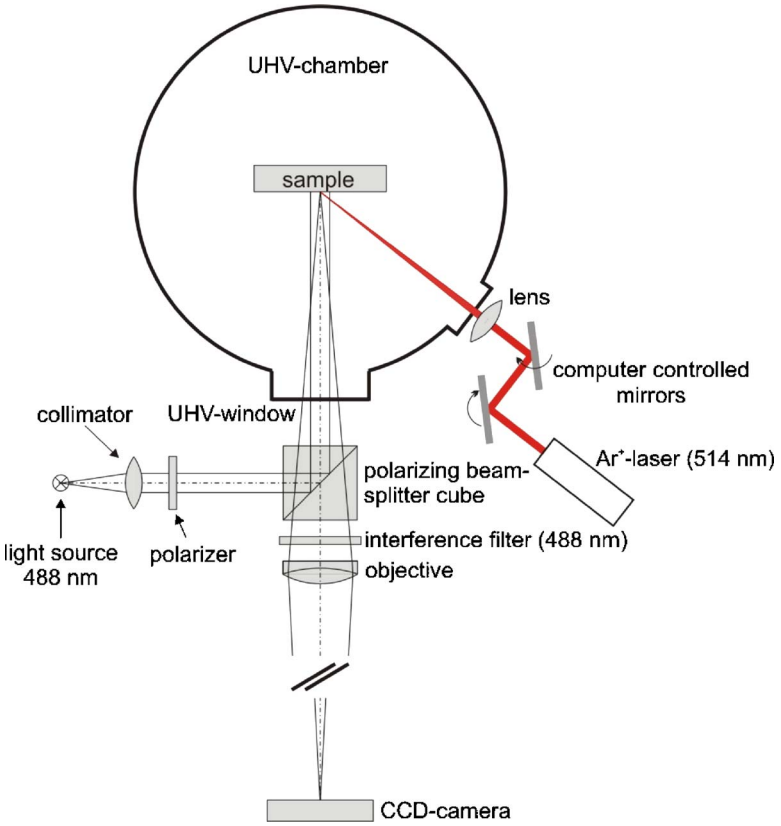

FIG. 9. (Color online) Schematic image of the experimental setup (not to scale). For details, see text.

IV. EXPERIMENTS

A. Experimental setup

In earlier experiments, propagating chemical waves had to be visualized in the presence of inert Ti boundaries [35,36]. These measurements were all performed using a photoemission electron microscope (PEEM), which has a sufficient lateral resolution and images the changes of the work function due to the adsorbed species. To achieve its high resolution, the sample has to be at a distance of 4 mm to the electron cathode lens, restricting severely any access to the surface and, in particular, preventing laser beam addressing.

At first glance, ellipsomicroscopy for surface imaging (EMSI) seems to be a more appropriate choice, since it leaves the whole surface totally open to additional experiments [25]. But EMSI relies on differences in adsorbed layer thickness. A microstructured surface features boundaries, laterally limiting the chemical waves, that are made out of Ti or similar metals and are several hundred angstroms tall. The signals from those boundaries would easily saturate the image, leaving no contrast to observe the reactive pattern formation. A different imaging method was therefore necessary, one that provided good contrast for the observation of the reaction dynamics, but which was preferably insensitive to the Ti microstructures. Additionally a sufficiently large working distance between the imaging instrument and the sample was necessary to allow for local addressing of surface activity by means of focused laser light.

Reflection anisotropy microscopy (RAM) conveniently combines the required properties. RAM has been extensively used to study CO oxidation on platinum. The first setup basically consisted of a classical ellipsometric configuration under almost normal incidence [25]. This setup was later improved by utilizing the intrinsic properties of a Foster prism and working under exactly normal incidence [37]. However, the spatial resolution of RAM (30 μm) was insufficient to image the relatively weak and thin reaction pulses presented in this paper. In order to improve the spatial resolution significantly, a new instrument was designed and built. Figure 9 shows a sketch of the experimental setup.

The Pt single crystal is located in an UHV chamber. As a light source for RAM, the 488 nm line of an Ar^+ laser is used. The laser light is collimated and afterwards polarized by means of a Glan-Thompson prism. The dielectric film within the polarizing beam splitter cube reflects about 99.9% of the incoming vertically prepolarized light onto the Pt sample. During reflection at the Pt(110) surface, the polarization may change depending on the coverage-dependent surface reconstruction [37]. The light propagates back to the beam splitter. The component with retained vertical polarization is reflected back to the light source. The other component which is polarized parallelly, due to interactions with the anisotropic Pt(110) surface, is transmitted and used for imaging of the crystal. Twice the light has to pass an UHV window. This window is specially designed to minimize stress-induced birefringence. The spatial resolution of this new setup is 8 μm. Thus, also thin pulses close to the limit of stability can now be observed with RAM. Through a second UHV window, the light of an additional Ar^+ laser (514 nm) can be focused onto the Pt surface. The position of the laser spot can be controlled via two computer-controlled galvanic mirrors. In order to remove unwanted 514 nm stray

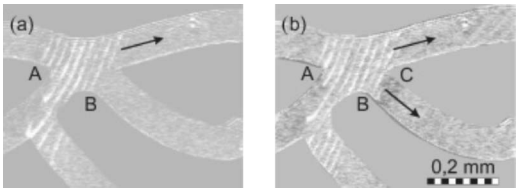

FIG. 10. Time-lapse images (an interval of 3 s between each two snapshots) showing a dying O-rich pulse "rescued" by a laser shot centered at *B*. The arrows indicate the propagation direction of the pulses. $T=455$ K, $P_{O_2}=2\times10^{-4}$ mbar, $P_{CO}=6.42\times10^{-5}$ mbar. (a) No laser shot is applied. The pulse decollates at *B* and enters the upper right channel. (b) A laser shot is applied for 50 ms with a power of 500 mW when the lower end of the pulse reaches point *B*. The pulse does not decollate at *B*, and splits into two at *C* entering both channels.

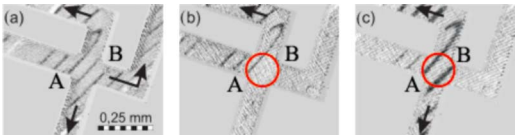

FIG. 11. (Color online) Guidance of CO-rich pulses in a labyrinthine structure. The circles indicate the location where the laser shot is applied. The laser shot duration is 1 s with a power of 230 mW, which destroys any part of the pulse within the circle. $T=451$ K, $P_{O_2}=2\times10^{-4}$ mbar, $P_{CO}=5.50\times10^{-5}$ mbar. (a) No laser shot is applied and the pulse enters all three channels. (b) A laser shot is applied when the lower end of the pulse is at corner *A* of the crossing. The pulse only enters the upper channel. (c) A laser shot is applied when the upper end of the pulse passes corner *B* of the crossing. The pulse is thus prevented from entering the channel on the right.

light from the RAM imaging path, a dielectric filter is used.

B. Experimental results

In the experiments, we were able to guide pulse propagation through different local laser heating protocols. We can assist the propagation of a pulse in the direction originally prohibited by the boundary curvature-induced instability through a short duration laser shot (Fig. 10); alternatively, we can apply excessive heating that actually destroys the pulses (Fig. 11).

In Fig. 10, an O-rich pulse is first ignited at the upper left channel and propagates toward the right. It is able to turn around corner *A*, but it decollates at corner *B* unless it is assisted by local laser shot. After applying a laser shot at the lower end of the pulse at *B*, the increase of local temperature reduces the CO coverage of the local CO-poisoned surface, which makes the adsorption of oxygen easier, so that the pulse is able to pass around the *B* corner [Fig. 10(b)].

If excessive heating is applied to a propagating CO-rich pulse, removing enough CO from the local surface, the pulse can be locally destroyed. In Fig. 11(b), we apply the laser heating for 1 s when the lower end of the pulse reaches corner *A* of the crossing. This erases the lower part of the pulse within the circle and prevents the pulse from entering the right and lower channels. In Fig. 11(c), we wait until the *upper end* of the pulse passes the *B* corner of the crossing before applying the laser heating. Only the pulse propagation in the right channel is thus obstructed.

V. SUMMARY AND CONCLUSIONS

Spontaneous pattern formation, and the dynamics of the resulting patterns in reacting systems, can be controlled at several levels. Designing the geometry of the catalytic domain, and using a galvanometer mirror-manipulated laser beam, we have demonstrated here through experiment and computation that the propagation of pulses in complex geometries can be guided, facilitated, or forbidden in real time. Sudden and intense boundary curvature changes can lead to a fundamental "decollation" instability; on the other hand, the laser-induced heating can either assist or prohibit pulse propagation depending on its intensity and location.

The combination of spatially fine-grained sensing with spatially fine-grained actuation opens up a wide array of possibilities in manipulating physical processes in complex microgeometries. Here we studied heterogeneous reacting systems; similar tools can be used to implement spatiotemporal networks in *homogeneous* reacting excitable media (e.g., Ref. [38]) or electrochemically reacting systems (e.g., Ref. [39]). Beyond chemically reacting systems, such tools are becoming increasingly useful—and used—in applications as diverse as droplet formation and mixing in microfluidics [40], directing cell migration [41], or manipulating coherent matter waves [42].

ACKNOWLEDGMENTS

This work was partially supported by an NSF/ITR grant and by AFOSR (I.G.K., L.Q.); L.Q. gratefully acknowledges the support of the U.S. DOE through PPPL. The authors also wish to acknowledge the experimental observations of rhomb constrictions in Michael Pollmann's thesis at the FHI.

[1] R. Jackson, J. Optim. Theory Appl. **31**, 1 (1980).
[2] J. Wolff, A. G. Papthanasiou, I. G. Kevrekidis, H. H. Rotermund, and G. Ertl, Science **294**, 134 (2001).
[3] A. G. Papathanasiou, J. Wolff, I. G. Kevrekidis, H. H. Rotermund, and G. Ertl, Chem. Phys. Lett. **358**, 407 (2002).
[4] X. Li, I. G. Kevrekidis, M. Pollmann, A. G. Papathanasiou, and H. H. Rotermund, Chaos **12**, 190 (2002).
[5] M. D. Graham, M. Bär, I. G. Kevrekidis, K. Asakura, J. Lauterbach, H. H. Rotermund, and G. Ertl, Phys. Rev. E **52**, 76 (1995).
[6] M. Bär, I. G. Kevrekidis, H. H. Rotermund, and G. Ertl, Phys. Rev. E **52**, R5739 (1995).

[7] G. Haas, M. Bär, I. G. Kevrekidis, P. B. Rasmussen, H. H. Rotermund, and G. Ertl, Phys. Rev. Lett. **75**, 3560 (1995).
[8] N. Hartmann, M. Bär, I. G. Kevrekidis, K. Krischer, and R. Imbihl, Phys. Rev. Lett. **76**, 1384 (1996).
[9] A. K. Bangia, M. Bär, I. G. Kevrekidis, M. D. Graham, H. H. Rotermund, and G. Ertl, Chem. Eng. Sci. **51**, 1757 (1996).
[10] M. Bär, A. K. Bangia, I. G. Kevrekidis, G. Haas, H. H. Rotermund, and G. Ertl, J. Phys. Chem. **100**, 19106 (1996).
[11] M. G. Zimmermann, S. O. Firle, M. A. Natiello, M. Hildebrand, M. Eiswirth, M. Bär, A. K. Bangia, and I. G. Kevrekidis, Physica D **110**, 92 (1997).
[12] S. Y. Shvartsman, E. Schütz, R. Imbihl, and I. G. Kevrekidis, Phys. Rev. Lett. **83**, 2857 (1999).
[13] N. Hartmann, I. G. Kevrekidis, and R. Imbihl, J. Chem. Phys. **112**, 6795 (2000).
[14] S. Y. Shvartsman, E. Schütz, R. Imbihl, and I. G. Kevrekidis, Catal. Today **70**, 301 (2001).
[15] J. P. Voroney, A. T. Lawniczak, and R. Kapral, Physica D **99**, 303 (1996).
[16] M. A. Liauw, J. Ning, and D. Luss, J. Chem. Phys. **104**, 5657 (1996).
[17] A. Lázár, H. D. Försterling, H. Farkas, P. Simon, A. Volford, and A. Noszticzius, Chaos **7**, 731 (1997).
[18] Á. Tóth and K. Showalter, J. Chem. Phys. **103**, 2058 (1995).
[19] E. M. Lucchetta, J. H. Lee, L. A. Fu, N. H. Patel, and R. F. Ismagilov, Nature (London) **434**, 1134 (2005).
[20] M. Joanicot and A. Ajdari, Science **309**, 887 (2005).
[21] R. Carretero-González, P. G. Kevrekidis, D. J. Framntzeskakis, and B. A. Malomed, Proc. SPIE **5930**, 125 (2005).
[22] T. Sakurai, E. Mihaliuk, F. Chirila, and K. Showalter, Science **296**, 2009 (2002).
[23] S. Q. Lima and G. Miesenböck, Cell **121**, 141 (2005).
[24] D. Grier, Nature (London) **424**, 810 (2003).
[25] H. H. Rotermund, G. Haas, R. U. Franz, R. M. Tromp, and G. Ertl, Science **270**, 608 (1995).
[26] K. Krischer, M. Eiswirth, and G. Ertl, J. Chem. Phys. **96**, 9161 (1992).
[27] E. G. Seebauer, A. C. F. Kong, and L. D. Schmidt, J. Chem. Phys. **88**, 6597 (1988).
[28] J. Wolff, A. G. Papathanasiou, H. H. Rotermund, G. Ertl, X. Li, and I. G. Kevrekidis, Phys. Rev. Lett. **90**, 018302 (2003).
[29] J. Cisternas, P. Holmes, I. G. Kevrekidis, and X. Li, J. Chem. Phys. **118**, 3312 (2003).
[30] M. Falcke, M. Bär, H. Engel, and M. Eiswirth, J. Chem. Phys. **97**, 4555 (1992).
[31] J. J. Tyson and J. P. Keener, Physica D **32**, 327 (1989).
[32] E. Meron, Phys. Rep. **218**, 1 (1992).
[33] L. Qiao, I. G. Kevrekidis, C. Punckt, and H. H. Rotermund, Phys. Rev. E (to be published), e-print nlin.PS/0512019.
[34] A. S. Mikhailov, *Foundations of Synergetics I: Distributed Active Systems* (Springer, New York, 1994).
[35] M. D. Graham, I. G. Kevrekidis, K. Asakura, J. Lauterbach, K. Krischer, H. H. Rotermund, and G. Ertl, Science **264**, 80 (1994).
[36] M. Pollmann, H. H. Rotermund, G. Ertl, X. Li, and I. G. Kevrekidis, Phys. Rev. Lett. **86**, 6038 (2001).
[37] J. Dicke, P. Erichsen, J. Wolff, and H. H. Rotermund, Surf. Sci. **462**, 90 (2000).
[38] M. Tinsley, J. Cui, F. V. Chirila, A. Taylor, S. Zhong, and K. Showalter, Phys. Rev. Lett. **95**, 038306 (2005).
[39] I. Z. Kiss, Y. M. Zhai, and J. L. Hudson, Science **296**, 1676 (2002).
[40] J. D. Tice, H. Song, A. D. Lyon, and R. F. Ismagilov, Langmuir **19**, 9127 (2003).
[41] X. Jiang, D. A. Bruzewicz, A. P. Wong, M. Piel, and G. M. Whitesides, Proc. Natl. Acad. Sci. U.S.A. **102**, 975 (2005).
[42] B. Eiermann, T. Anker, M. Albiez, M. Taglieber, P. Treutlein, K.-P. Marzlin, and M. K. Oberthaler, Phys. Rev. Lett. **92**, 230401 (2004).